Regional Comparison of GOES Cloud-Top Properties and Radar Characteristics in Advance of First-Flash Lightning Initiation

JOHN R. MECIKALSKI, XUANLI LI, AND LAWRENCE D. CAREY

Department of Atmospheric Science, University of Alabama in Huntsville, Huntsville, Alabama

EUGENE W. MCCAUL JR.

Universities Space Research Association, Huntsville, Alabama

TIMOTHY A. COLEMAN

Department of Atmospheric Science, University of Alabama in Huntsville, Huntsville, Alabama

(Manuscript received 17 April 2012, in final form 28 June 2012)

ABSTRACT

Lightning initiation (LI) events over Florida and Oklahoma are examined and statistically compared to understand the behavior of observed radar and infrared satellite interest fields (IFs) in the 75-min time frame surrounding LI. Lightning initiation is defined as the time of the first lightning, of any kind, generated in a cumulonimbus cloud. Geostationary Operational Environmental Satellite (GOES) infrared IFs, contoured frequency by altitude diagrams (CFADs) of radar reflectivity, and model sounding data, analyzed in concert, show the mean characteristics over time for 36 and 23 LI events over Florida and Oklahoma, respectively. CFADs indicate that radar echoes formed 60 min before Florida LI, yet Oklahoma storms exhibited a ~30-min delayed development. Large ice volumes in Florida developed from the freezing of lofted liquid hydrometeors formed by long-lived (~45 min) warm rain processes, which are mostly absent in Oklahoma. However, ice volumes developed abruptly in Oklahoma storms despite missing a significant warm rain component. GOES fields were significantly different before 30 min prior to LI between the two locations. Compared to Florida storms, lower precipitable water (PW), higher convective available potential energy, and higher 3.9-μm reflectance in Oklahoma, suggest stronger and drier updrafts producing a greater abundance of small ice particles. Somewhat larger 15-min 10.7-μm cooling rates in Oklahoma confirm stronger updrafts, while clouds in the 60–30-min pre-LI period show more IF variability (e.g., in the 6.5–10.7-μm difference). Florida storms (high PW, slower growth) offer more lead time for LI predictability, compared to Oklahoma storms (low PW, explosive growth), with defined anvils being obvious at the time of LI.

1. Introduction

The main motivation for this study is the lack of previous research linking observations from ground-based radar, lightning, and geostationary satellite for convective clouds, [in this case, developing cumulus clouds undergoing convective initiation (CI)] and first-flash lightning initiation (LI) processes. Specifically, this paper presents an analysis in which contoured frequency by altitude diagrams (CFADs) were developed for a population of storms over the period 60 min prior to 15 min after LI, in two distinct geographical regions: Florida (FL) and Oklahoma (OK). The evolution of the CFAD of reflectivity (Z) data is then compared to time series of cloud-top geostationary satellite-based infrared (IR) observations that describe physical attributes of cumulus cloud dynamics (i.e., updraft strength, updraft width, glaciation, and cloud depth). For this research, LI is defined as the first detectable lightning flash [of any type, not just cloud-to-ground (CG)] from a new, growing cumulus cloud. The purpose of this analysis is to increase understanding on how cumulus clouds and precipitation evolve over a 75-min time frame with

Corresponding author address: John R. Mecikalski, University of Alabama in Huntsville, Atmospheric Sciences, NSSTC, 320 Sparkman Drive, Huntsville, AL 35805.
E-mail: johnm@nsstc.uah.edu

DOI: 10.1175/MWR-D-12-00120.1

TABLE 1. The convective initiation (CI) and lightning initiation (LI) interest fields, and their respective thresholds, used in Mecikalski and Bedka (2006) and H10. The last column summarizes each field's physical description.

Interest field	Critical CI value (Mecikalski and Bedka 2006)	15–30-min threshold (H10)	Physical description
10.7-μm T_B	<0°C	<0°C	Cloud tops cold enough to support super-cooled water and ice mass growth; cloud-top glaciation
10.7-μm T_B time trends	<-4°C (15 min)$^{-1}$ [ΔT_B (30 min)$^{-1} < \Delta T_B$ (15 min)$^{-1}$]	<-6°C (15 min)$^{-1}$	Cloud growth rate (vertical)
Timing of 10.7-μm T_B drop below 0°C	Within prior 30 min	Not used	Cloud-top glaciation
6.5–10.7-μm T_B difference	T_B diff: -35° to -10°C	>-30°C	Cloud-top height relative to mid/upper troposphere
13.3–10.7-μm T_B difference	T_B diff: -25° to -5°C	>-13°C	Cloud-top height relative to mid/upper troposphere; better indicator of early cumulus development but sensitive to cirrus
6.5–10.7-μm T_B time trend	>3°C (15 min)$^{-1}$	>5°C (15 min)$^{-1}$	Cloud growth rate (vertical) toward dry air aloft
13.3–10.7-μm T_B time trend	>3°C (15 min)$^{-1}$	>4°C (15 min)$^{-1}$	Cloud growth rate (vertical) toward dry air aloft
3.9–10.7-μm T_B difference	Not used	>17°C	Cloud-top glaciation
3.9–10.7-μm T_B time trend	Not used	>1.5°C (15 min)$^{-1}$	Sharp decrease, then increase indicates cloud-top glaciation
3.9-μm fraction reflectance	Not used	<0.11	Cloud top consists of ice (ice is poorer reflector than water at 3.9 μm)
3.9-μm fraction reflectance trend[3]	Not used	<-0.02 (15 min)$^{-1}$	Cloud-top glaciation rate

respect to LI, when radar CFAD and Geostationary Operational Environmental Satellite (GOES) IR fields are considered in tandem. A further goal will be to gain insight into the predictability of LI, from a combined satellite and radar perspective.

In a previous study, Harris et al. (2010; hereafter H10; see also Siewert 2008), the goals were to gain an understanding of the behavior of *only* GOES-sensed IR cloud-top properties for cumulus clouds that grow and form an initial lightning flash, to statistically quantify satellite field importance related to LI, and to suggest preliminary ''critical'' values per field. H10 analyzed the behavior of 10 *GOES-12* IR interest fields (IFs) within 1 h prior to LI for 172 thunderstorms in four different regions: FL; OK; Washington, D.C.; and northern Alabama. Statistical analysis revealed that 8 of the 10 IFs (Table 1) exhibited predictive capability for nowcasting LI, with an average forecast lead time of 35 min.

The present study extends H10. Cumulus cloud processes, inferred from GOES IR IFs, are analyzed in concert with precipitation (specifically, Z) data from the National Weather Service Weather Surveillance Radar-1988 Doppler (WSR-88D). This is done to build understanding and to quantify the precursors to LI in *both* IR and Z fields, simultaneously. The comparisons are evaluated statistically to determine, over the 75 min surrounding LI, when the IR and Z patterns are (or are not) significantly different between FL and OK. Variations of environmental factors affect the kinematic and microphysical characteristics that influence the charging process, the physics involved in LI occurrence, and (perhaps) how much lightning is eventually produced in the cumulonimbus clouds (which is only an inference from this research). This study then relates differences in convective cloud processes, found between FL and OK, to variations in the stability, thermodynamic (temperature and moisture profiles), and boundary layer characteristics. Quantifying the behavior of geostationary IR and Z data, for growing cumulus and cumulonimbus clouds, is novel in that it simultaneously helps toward predicting LI and lightning in general. Past research is subsequently drawn in toward explaining relationships observed within both the CFAD and GOES IR datasets.

2. Background

Thunderstorm electrification has long been discussed (Wilson 1916; Simpson and Scrase 1937), and yet it is still not completely understood owing to the dynamic and microphysical processes across multiple scales involved, the complex interactions among them (Williams

1988), and the difficulty of obtaining in situ observations within vigorous convective storms. It is believed that precipitation-based charging theories are the primary mechanism for thunderstorm electrification (Dye et al. 1988, 1989; MacGorman and Rust 1998). The precipitation-centered charging theories fall into two categories: the inductive charging mechanisms (Elster and Geitel 1913; Aufdermauer and Johnson 1972) and the ice particle collision-based charging mechanisms (also referred to as ''non-inductive'' charging; Workman and Reynolds 1949; Rutledge et al. 1992; Helsdon et al. 2002; Mitzeva et al. 2005; Emersic and Saunders 2010). Rebounding collisions, between riming graupel (or hail particles) and ice crystals in the presence of super-cooled liquid water, is central to the non-inductive charging theory. Supported by field evidence, laboratory results, and model results, the non-inductive mechanism is the favored dominant charging theory (Williams and Lhermitte 1983; Takahashi 1978; Mansell et al. 2005).

Ground-based radar Z data were used in numerous studies to help understand the mechanism of thunderstorm electrification and lightning activity (Buechler and Goodman 1990; Michimoto 1993; Gremillion and Orville 1999; Vincent et al. 2004). Since strong Z values are often observed in mixed-phase regions of clouds, they can indicate the existence of large dense ice such as graupel and hail. Hence, their existence has been widely used as an indicator in studies of nowcasting the onset of CG lightning (Dye et al. 1989; Buechler and Goodman 1990; Hondl and Eilts 1994), total lightning frequency (Petersen and Rutledge 2001; Deierling and Petersen 2008; Xu et al. 2009; Liu et al. 2010), and lightning cessation (Hinson 1997; Wolf 2007; Stano et al. 2010; Anderson 2010). A common scenario demonstrated in previous radar-based studies is a lag time, on the order of 10 min, between the appearance of a large Z (e.g., 30–40 dBZ) at temperatures below a certain threshold (e.g., from 0° to −20°C) and a first CG lightning strike. For example, Dye et al. (1989) studied thunderstorms in New Mexico and identified a relationship between CG flash onset and the occurrence of 40 dBZ reaching −10°C with cloud tops exceeding 9.5-km altitude. Michimoto (1991) found that the first CG lightning discharge occurred 5 min after 30 dBZ reached the −20°C level. Hondl and Eilts (1994) found that, from 28 thunderstorms in FL, a 10-dBZ echo near the freezing level is an indicator of a developing thunderstorm. Vincent et al. (2004) examined different sets of criteria for 50 thunderstorm cases from September 2001 to June 2002. They concluded that a 40-dBZ echo at −10°C gives a 100% probability of the detection of LI, with an average lead time of 14.7 min. Yang and King (2010) indicated that the best predictor for nowcasting the onset of CG lightning in Canada is a 40-dBZ echo at the −10°C level, with an average lead time of 17 min. Similar to Hondl and Eilts (1994), Seroka et al. (2012) examined summertime lightning activity and found that the best index for CG flash initiation is a 25-dBZ echo at −20°C, and 25 dBZ at –15°C for intracloud (IC) flash initiation. Wolf (2007) examined 1100 positive convective cells in radar data, finding an average lead time to first lightning of 5–10 min. The most comprehensive radar-based study (based on sample size), Mosier et al. (2011; 67 000 positive convective storm cells), determined an average lead time for LI of 10–13 min.

Geostationary satellite data have shown their usefulness for nowcasting the development of severe storms and estimating storm intensity with CG flash rates (Goodman et al. 1988; Roohr and Vonder Haar 1994; Roberts and Rutledge 2003). Mecikalski and Bedka (2006) and Mecikalski et al. (2008) evaluated the behavior of eight GOES IR IFs, and defined threshold values as precursors to 0–1-h CI (the first occurrence of a ≥35-dBZ radar echo at the −10°C altitude; Browning and Atlas 1965; Wilson and Schreiber 1986; Wilson et al. 1992). Mecikalski et al. (2010a,b) extended this work to the Meteosat Second Generation (MSG), which offers more spectral information than GOES, to more clearly identify physical processes such as cloud-top glaciation, an important proxy indicator for where the non-inductive charging process may be occurring in cumulus clouds. H10 represents a parallel effort to Mecikalski and Bedka (2006), yet focuses on the use of 3.9-μm reflectance from GOES (in addition to other IR fields) to infer locations of cumulus cloud with significant updrafts that are glaciating at the cloud top (i.e., possess ongoing non-inductive charging).

Given the typical time and evolution scales of convective clouds undergoing CI and LI (≤2 h), the research presented in this paper differs from the extensive work done using Tropical Rainfall Measuring Mission (TRMM; e.g., Cecil and Zipser 2002; Liu et al. 2008) data, which cannot consider 0–2-h time-evolution aspects of cumulus cloud development, yet which utilize similar combinations of data (radar, lightning, and passive microwave remote sensing). A brief review shows that many previous studies combined TRMM Precipitation Radar (PR), Microwave Imager (TMI), and Lightning Imaging Sensor (LIS) products to quantify relationships between convective rainfall, cloud microphysics, and electrification (Boccippio et al. 2000; Petersen and Rutledge 2001; Cecil and Zipser 2002; Del Genio and Kovari 2002; Petersen et al. 2002; Cecil et al. 2005; Liu et al. 2008, 2010). Toracinta et al. (2002) observed a higher probability of lightning in tropical continental features than tropical oceanic features. They found

that the lightning flash rate increases with decreasing TRMM 85- and 37-GHz brightness temperatures (T_B) and increasing midlevel PR Z. Petersen et al. (2005) suggested the relationship between precipitation ice-water path and lightning flash density, which indicates that cloud electrification increases with ice mass. Katsanos et al. (2007) found higher ratios of CG lightning to total lightning activity for ''colder'' TRMM 85-GHz microwave polarization corrected T_B. They also found higher mean and maximum Z profiles collocated with lightning versus without lightning. Pessi and Businger (2009) showed that Z in the mixed-phase region increases significantly with lightning rate, while the lapse rate of Z decreases. They noted that the heights of the echo tops show a strong logarithmic correlation with lightning rate. As noted, for the present study, one goal is to identify similar relationships, but between cloud-top IR observations collected from GOES together with WSR-88D observations, using understood relationships on how developing CI and LI events appear in each dataset separately.

Radar studies, using dual-polarimetric (DP) techniques for hydrometeor identification, have confirmed key aspects of the Z-only studies. Total lightning is highly correlated with the DP radar-inferred graupel/hail volumes (Carey and Rutledge 1996), and graupel/hail ice mass (Carey and Rutledge 2000). Deierling et al. (2008) further demonstrated that the DP radar-inferred ice mass flux explains most of the variability seen in the total lightning flash rates. Woodard et al. (2012) recently demonstrated that Z-only and DP-based radar techniques for operational LI forecasting have very similar performances. Although DP radar data were not available for this study, the consistency between other DP-based and Z-only radar studies of lightning gives us confidence in using Z observations for inferring key microphysical processes relevant to LI. Ongoing research, comparing DP radar- and satellite IR-inferred physical trends for lightning and non-lightning storms, will be presented in a follow-on paper.

Beyond a description of the data and processing methodology in section 3, section 4 presents the main results. The study's findings are discussed, and conclusions are presented, in section 5.

3. Data processing methodology

The three main datasets used in this study include lightning observations from the Lightning Mapping Array (LMA) network and 4D Lightning Surveillance System (4DLSS), WSR-88D Z within the National Mosaic and Multisensor QPE (NMQ) dataset, and *GOES-12* IR fields. Details on the LMA and *GOES-12* IR field processing are found in H10, beyond what is described below.

a. Lightning data and GOES interest fields

Central Oklahoma Lightning Mapping Array (OKLMA) data were used to identify LI events for the OK storms in the summer of 2009. The LMA is a mesoscale network of Global Positioning System (GPS) time-of-arrival sensors that detect very high-frequency (VHF) signals (Krehbiel et al. 2000). The array spans 60 km $\times$ 80 km horizontally to detect time and three-dimensional (3D) spatial locations of lightning sources. The OKLMA has 11 GPS VHF receivers south and west of Oklahoma City to sense lightning source radiation in the 54–88-MHz range. The LMA flash-grouping algorithm, developed at the National Space Science Technology Center at the University of Alabama in Huntsville (McCaul et al. 2009), was used to compute the time, latitude, longitude, and altitude of the initiation point of flashes. The 4DLSS data at the Kennedy Space Center (KSC) are used to examine lightning activity for the FL storms. The 4DLSS includes both a CG and a total cloud lightning (combined cloud-to-cloud, cloud-to-air, CG and IC lightning) sensor array. The 4DLSS data were processed and obtained from the National Aeronautics and Space Administration (NASA). The 4DLSS array also uses VHF and time-of-arrival techniques to locate lightning sources. The array has 9 VHF sensors in the 60–66-MHz range distributed across a 45 km $\times$ 65 km horizontal coverage area. The 4DLSS data are clustered using the Nelson (2002) flash–grouping algorithm, as refined by Murphy et al. (2008).

A valid ''flash,'' in both the OKLMA and 4DLSS datasets, is defined as a lightning flash that has at least four sources. In many past studies, LI is often defined as the first CG flash, largely due to the data availability (Gremillion and Orville 1999; Vincent et al. 2004; Mosier et al. 2011). In this study, as the total lightning data were collected, LI is defined as the time of the first flash, which could be either IC, cloud-to-cloud, cloud-to-air, or CG. Hence, the use of the OKLMA and the 4DLSS data enable us to examine the total lightning activity and to make a more accurate and complete inspection of the lightning initiation process (Steiger et al. 2007a,b). Examination of total lightning (including CG and IC flashes) not only benefits the understanding of the kinematic and microphysical processes related to lightning activity but also has practical applications in lightning warning product development especially for aviation operations.

The *GOES-12* imagery was aligned with the OKLMA and 4DLSS lightning data to find potential LI events through subjective comparison and selection. GOES

data from four channels were examined: 3.9, 6.5, 10.7, and 13.3 μm. The IR imagery has a resolution of 8 km for the 13.3-μm channel and 4 km for all other channels (Menzel and Purdom 1994). H10 (see also Mecikalski and Bedka 2006) explored the physical attributes of growing cumulus clouds for LI with 10 IR IFs: the 10.7-μm T_B, the 15-min 10.7-μm T_B trend, the 6.5–10.7-μm T_B difference, the 15-min 6.5–10.7-μm T_B difference trend, the 3.9–10.7-μm T_B difference, the 15-min 3.9–10.7-μm T_B difference trend, the 13.3–10.7-μm T_B difference, the 15-min 13.3–10.7-μm T_B difference trend, the 3.9-μm reflectance, and the 15-min 3.9-μm reflectance trend. Table 1 summarizes the physical characteristics of the IFs that were employed in H10. Although only 8 of the 10 IFs were found to contain unique information for LI prediction (e.g., the 15-min 3.9–10.7-μm trend and the 3.9-μm reflectance trend fields contained little unique information), this study evaluated all 10 IFs in light of the CFAD analysis.

GOES typically has a 15-min time collection interval, and events were tracked from 60 min in advance of LI to 15 min after LI. Therefore, GOES IFs at 60 min (−60 min), 45 min (−45 min), 30 min (−30 min), 15 min (−15 min) *before* LI, at the time of LI (LI), and at 15 min *after* LI (+15 min) are used. For each LI event, a storm's coldest 10.7-μm T_B is tracked over 75 min as a means of focusing on the main updraft in a developing cumulus (cumulonimbus) cloud.

b. Radar data

The 3D mosaic *Z* fields from the NMQ system (Zhang et al. 2006, 2011) were obtained from the National Severe Storms Laboratory (NSSL). The 3D *Z* field is a seamless high-resolution national radar mosaic developed from ~140 WSR-88D radars in the continental United States and 31 C-band weather radars in southern Canada. The NMQ grid covers the region from 20°–55°N to 130°–60°W, with a constant horizontal resolution of 1 km × 1 km, updated every 5 min. The *Z* data have 31 vertical levels from 500 m to 18 km above mean sea level (MSL). The vertical resolution is 0.25 km below 3 km MSL, 0.5 km between 3 and 9 km MSL, and 1 km above 9 km MSL. The potential LI cases identified from the *GOES-12* IR and lightning fields were tracked manually in *Z* images to collocate each storm with the corresponding one observed from the satellite observation. The NMQ *Z* were examined every 15 min near the satellite observational time. Since the GOES data only examine the ~100-m-thick cloud-top layer, valid LI cases are narrowed down to those that can be clearly tracked in both radar and IR data without interactions with neighboring storms.

TABLE 2. Times (UTC) and dates of Oklahoma (OK) and Florida (FL) storms.

	Date	No. of storms and times of LI
Oklahoma	25 May 2009	[1] 1753
	27 Jun 2009	[1] 2141
	30 Jun 2009	[6] 1954, 1956, 2023, 2040, 2033, 2055
	1 Jul 2009	[9] 2055, 2101, 2132, 2222, 2223, 2242, 2300, 2309, 2332
	16 Jul 2009	[5] 1903, 1935, 2014, 2052, 2059
	10 Aug 2009	[1] 1959
Florida	2 Jun 2009	[5] 1512, 1543, 1615, 1654, 1729
	15 Jun 2009	[4] 1737, 1738, 1844, 2000
	26 Jun 2009	[4] 1450, 1600, 1658, 1741
	12 Jul 2009	[4] 1942, 2013, 2014, 2208
	18 Jul 2009	[3] 1635, 1703, 1712
	29 Jul 2009	[3] 1728, 1939, 2029
	30 Jul 2009	[4] 1613, 1842, 1829, 1927
	19 Aug 2009	[4] 1401, 1553, 1554, 1728
	21 Aug 2009	[4] 1645, 1705, 1753, 1814
	23 Aug 2009	[1] 1638

c. Case selection

As detailed in H10, summertime lightning–producing storms from May to August 2009 were examined for potential cases. Good lightning observations are limited to locations within 100–150 km from the OKLMA and 4DLSS array centers because the accuracy and efficiency of flash detection decreases with distance. Since *GOES-12* 3.9-μm reflectance will be most usable when the solar zenith angle is ≤68° (Lindsey et al. 2006), LI cases occurring between 1351 and 2315 UTC in OK and between 1242 and 2208 UTC in FL were evaluated. Storms overlaid by cirrus clouds were removed because even thin cirrus above cumulus clouds produce unrepresentative colder cloud-top T_B values, degrading the properties that can be estimated from the GOES data. Next, the LI events selected from *GOES-12* imagery were tracked manually in radar *Z* fields. Radar *Z* images were used to remove the cases that developed from, mixed with, or merged into nearby preexisting storms. Also, when storms move within 30 km of a radar site, *Z* might be underestimated as part of a storm will be in the radar's "cone of silence." Therefore, these cases were eliminated. In the end, a total of 36 LI events in FL and 23 in OK were identified. Table 2 lists the dates of the FL and OK storms with the times of LI.

d. Contoured frequency by altitude diagram formation

The CFAD is a contour plot displaying the frequency distribution of *Z* in an area of detectable echoes at each height. Many studies (e.g., Wang and Carey 2005; Cecil 2011) show that the CFAD is a convenient tool to examine the characteristics of storms, especially for their

temporal evolution. Here, CFADs are calculated according to Yuter and Houze (1995). The creation of a CFAD begins with a histogram calculation using a constant Z bin width within a constant vertical volume. Here, the Z bin width is set as 4 dBZ and the vertical interval is 0.5 km. Then the histograms are normalized with the total number of points at each vertical level, and the results are multiplied by 100 to present the fraction as a percentage value. The CFAD ignores the horizontal echo structure and summarizes the frequency distribution information in a 2D plot. The line labels, within a given CFAD shown here, are the percentage fraction of the frequency Z distribution per level (dBZ^{-1} km^{-1}). In this study, a CFAD for each individual storm was first calculated, and then the average of the CFADs for all FL and OK storms were compared at the defined times (-60, -45, -30, -15, 0, and $+15$ min). These averaged per time CFAD analyses will show the evolution of the statistical characteristics of the LI events from a radar perspective, to correspond to the *GOES-12* datasets, and at the same time will be done in way that statistically compares FL and OK LI events.

e. Rapid Update Cycle model soundings

To address the differences in the CFAD and GOES IF datasets between FL and OK, ''representative'' afternoon (0000 UTC) soundings were studied to obtain a clearer view of cloud processes that contributed to LI. Parameters considered include precipitable water (PW), boundary layer depth, lifted condensation level (LCL), level of free convection (LFC), freezing level (FRZLVL), convective inhibition (CIN), and mean layer convective available potential energy (CAPE) as a measure of instability. Soundings were collected from 13-km resolution Rapid Update Cycle (RUC) initialization (0-h analyses) grids since the sparse radiosonde network often failed to capture temperature and moisture profiles near the LI events. The General Meteorological Package (GEMPAK; desJardins et al. 1991) *nsharp* application was used to analyze the RUC data. For example, the 0000 UTC sounding at Oklahoma City, OK, was often located to the west of the main surface moisture that supported thunderstorm development, and hence did not relate to the prestorm environment very well. Sounding data are useful for gaining insight into some of the signals seen in the satellite observations, particularly those related to 1) updraft widths as a function of boundary layer depth, 2) updraft velocities related to instability or CAPE values, 3) updraft hydrometeor characteristics related to CAPE and PW, and 4) confirmation of warm rain processes at early stages in cloud development, especially over FL (as noted above) related to LCL and FRZLVL.

f. Statistical significance testing

All results are shown in a manner that facilitates easy comparison between FL and OK events, specifically, with both locations shown side-by-side per time. To quantify statistical significance, and to increase the value of the interpreted results, comparisons of Z and IR IFs are shown in ''box and whiskers'' or box plots (Wilks 2011, 29–33), which qualitatively assess each field's uniqueness per 15-min interval. Each box plot has a notched box representing the middle 50%, or interquartile range (IQR), of the data. Higher spread, and therefore higher data variability, is associated with a larger IQR. The horizontal line in the notch's center represents the median value. The vertical dashed lines on either side of the IQR (the whiskers) represent ~99% of a distribution from whisker to whisker (top and bottom horizontal lines). Any open circles beyond the whiskers signify outlier data points. Importantly, the notch within each box plot's IQR represents a visual statistical significance test. Notch overlap verifies whether each dataset (for a given time) is (or is not) significantly different than another at the $\alpha = 0.05$ significance level. As the most common α threshold, the 5% test level allows one to accept that the notch-overlap hypothesis test is incorrectly assessing the results $\leq$5% of the time. If the notches do not overlap (e.g., the 10.7-μm T_B at -15 min, FL vs OK) then the two datasets are deemed significantly different at the 95% confidence level.

4. Results

a. CFADs and radar reflectivity in OK and FL

Figure 1 shows that the FL storms possess larger Z values overall, suggesting that they contain more moisture (in terms of precipitation water and ice volumes) than the OK storms before and at LI. At LI, the CFAD of 40 dBZ at the low troposphere (below the 3-km level) reaches 2.5% dBZ^{-1} km^{-1} for FL storms, which is higher than that for OK storms (Fig. 1b). Also, by LI the echo tops are around 18 km for the FL storms, compared to 15 km in OK. The echo top in our analysis is defined as the uppermost height of the 18-dBZ echo (in the NMQ data). The mean Z is around 24 dBZ in low- to midtroposphere levels of FL cases at the LI time, which is 4 dBZ higher than that for the OK cases. Overall, FL storms show a sharper decrease in mean Z (red line) from 3–10 km than OK events, indicating a larger fraction of higher low-level Z.

The FL storms develop earlier but possess steadier or slower development rates when compared to the OK storms. Despite slow initial growth before -30 min, the OK storms show faster echo-top growth, and hence

more explosive intensity changes, with development instead concentrated within the last 30 min before LI. Specifically, a strong echo convective core (30–40 dBZ at 2–4-km altitude, on average) in FL storms is already found in the −45- and −30-min time frame. The echo top in CFADs of the FL storms reaches 15 km at −45 min, whereas the OK storms do not exceed 15 km until LI. The occurrence of 40 dBZ in FL storms reaches 1% dBZ^{-1} km^{-1} at low- to midtroposphere at −30 min, while for OK storms, the occurrence of 40 dBZ does not reach 1% dBZ^{-1} km^{-1} until LI. The maximum of mean-Z profile is near 15 dBZ at −45 min for the FL storms, while in comparison, the maximum of mean Z reaches only 12 dBZ at −15 min in OK storms. Again, this implies that the OK storms have more rapid development, mainly within the 30 min before LI. At LI, the difference in high Z (>30 dBZ) at upper levels between the FL and OK cases is much smaller than that at −45, −30, or −15 min.

The shape of the CFAD profiles offers additional information on storm structure. In FL, from −30 to −15 min, a larger percentage (>7.5% dBZ^{-1} km^{-1}) of 7–15-dBZ values are seen below 5 km (below the freezing level), oriented with a positive slope, which implies the presence of small raindrops reaching to low altitude. These patterns are not seen in OK, which is in a drier environment (i.e., evaporation of small hydrometers) with higher cloud bases. The core of maximum Z frequency is mainly vertically aligned above 5 km in both the FL and OK storms, reaching maximum values of 10%–12% dBZ^{-1} km^{-1}. However, in stark contrast to FL events, this vertical alignment switches to a negative slope in the OK storms from ~10.5 to near 15 km (reaching maximum values >15% dBZ^{-1} km^{-1} at 12.5 km), which indicates the presence of a large amount of small ice particles at cloud top. More discussion on the relevance of this small ice at cloud top will be given below related to *GOES-12* IF interpretation.

The slope of the tails of the CFADs (i.e., 2.5% dBZ^{-1} km^{-1} and 1% dBZ^{-1} km^{-1} lines in Fig. 1) just prior to LI (−15 to LI) are noticeably different in OK and FL from the freezing level up through the mixed phase zone at midlevels (4.5–8 km). The tails of the OK CFAD are more vertical than FL, or possess a slower drop off of the tail in the OK Z distribution with height through the mixed phase zone. In contrast, the tails of the FL Z distribution decrease more rapidly from the freezing level up to 8 km. The Z drop off with height is again suggestive of a more dominant warm rain and associated coalescence–freezing process in FL for the generation of precipitation-sized ice. Additionally, the difference in the slope of the tails, of the CFADs at midlevels just prior to and including LI, also suggests a more rapid and robust riming and hail production process at midlevels in OK.

Figure 2 again shows that OK storms develop much more in the 30 min before LI, as compared to the FL events. The maximum Z of OK storms increases from 6 dBZ at −30 min to 20 dBZ at −15 min, and to 44 dBZ at LI. The FL storms show a slower increase of maximum Z from 35 dBZ at −30 min to 45 dBZ at −15 min, then to 52 dBZ at LI. Despite the more rapid growth in OK, when LI occurs the FL storms have a stronger maximum Z than the OK cases (51 vs 44 dBZ), and a sharper decrease of Z from 5–8 km This suggests weaker updrafts in FL versus in OK storms (see Zipser and Lutz 1994). After LI, the Z maximum in OK exceeds that in FL, suggesting the presence of hail.

The results in Fig. 3 corroborate those in Figs. 1a,b showing that only smaller, less rapidly developing cumulus clouds possessing small-sized (<10 μm; undetectable by S-band WSR-88D radar) drops, dominate conditions at −60 to −15 min in OK. In FL, a lower percentage of 0–5-dBZ echoes compared to in OK at −60 min suggest the presence of small clouds. However, these FL clouds quickly come to be filled with larger drops by −45 min and beyond (higher Z values), and the early development of warm rain processes (Nelson 1971; Ogura and Takahash 1973; Lau and Wu 2003). These result do not provide insight into why hydrometeor sizes remain low in OK clouds, which could be the result of very few clouds, high aerosol contents that keep hydrometeors small (e.g., Khain et al. 2005), or stronger updrafts and short growth periods for in-cloud particles (Rosenfeld and Lensky 1998). More will be said on this topic when environmental and stability parameters are analyzed. By −15 to +15 min, the frequency plots begin to look similar, which compares well to the CFADs (Fig. 1), especially at LI and +15 min.

Like Fig. 3, Figs. 4a–c show that FL and OK growing cumulus clouds are quite different until the time of LI and at +15 min, when the distributions of radar-derived parameters overlap. Specifically, the box-and-whiskers plot overlap at these two times for echo top (Fig. 4a) and maximum height of the 30-dBZ echo (Fig. 4c), confirming they are statistically similar datasets. The maximum Z field (Fig. 4b) is only similar in FL and OK at +15 min.

b. GOES interest field variability

These radar results are next considered in light of GOES cloud-top IR fields, focusing on physical processes, while comparing the FL and OK events. The behavior in the GOES IFs, as a function of time between FL and OK, are shown in Figs. 5a–d and 6a–f, with box-and-whiskers plots used to establish statistical significance of dataset differences.

The 10.7-μm T_B (Fig. 5a) and its time trend (i.e., ''cloud-top cooling rates''; Fig. 6a) provide good

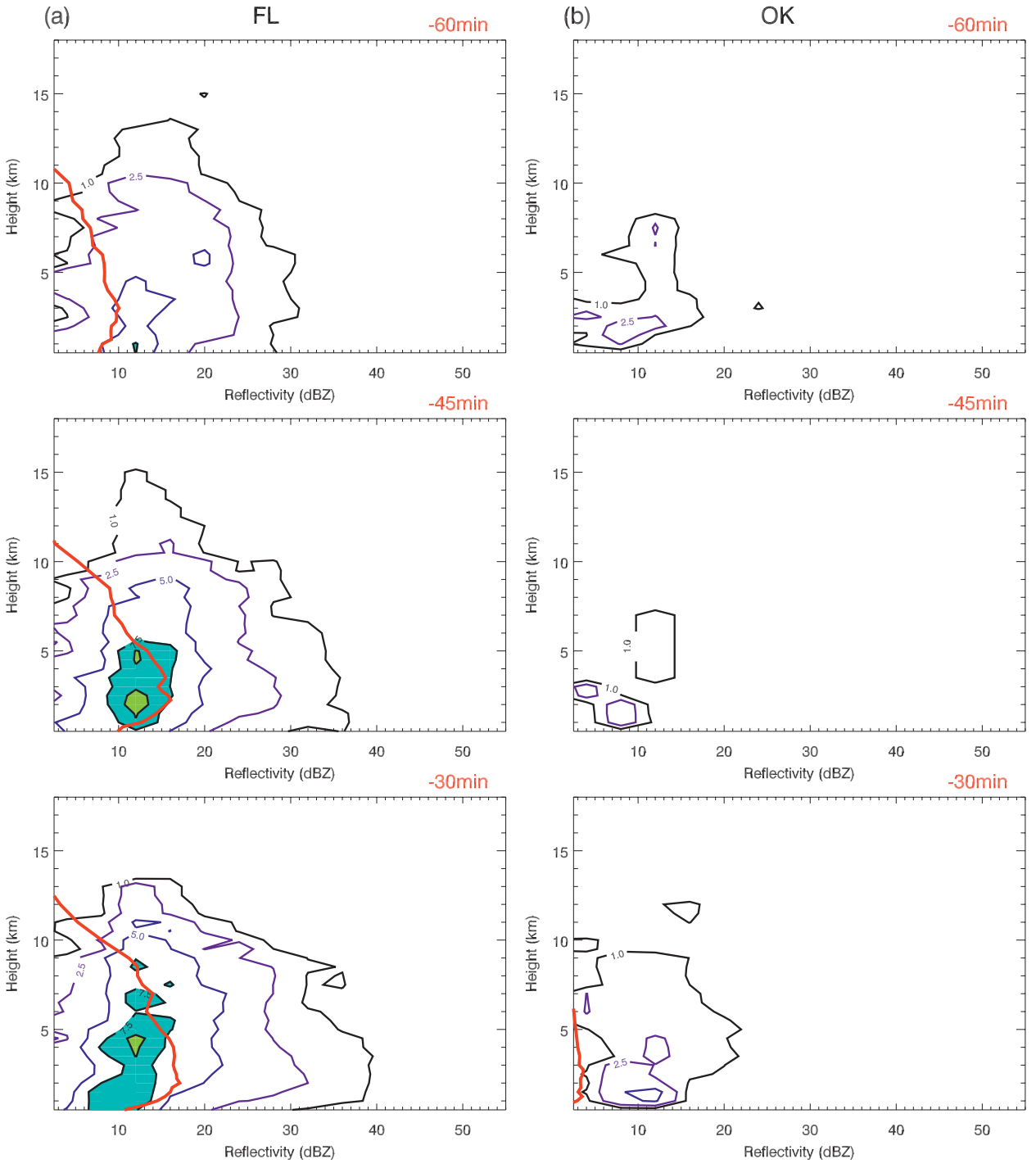

FIG. 1. CFAD plots, from 60 min before (−60 min) to 15 min after (+15 min) LI, for (a) 36 storms in FL and (b) 23 storms in OK. The bin size is 4 dBZ and the vertical resolution is 0.5 km. The thick red line shows the profile of mean reflectivity. The line labels are the percentage fraction of the frequency reflectivity distribution per level. See text for interpretation.

information toward understanding the processes related to LI occurring within OK and FL events. Cloud growth in OK is indicated to be more rapid compared to FL between −60 and −15 min. Median cloud-top cooling rates in OK were between −5°C (15 min)$^{-1}$ and −10°C (15 min)$^{-1}$, versus −3°C (15 min)$^{-1}$ and −8°C (15 min)$^{-1}$ in FL. The FL storms developed to a higher altitude overall, as confirmed by lower values of 10.7-μm T_B,

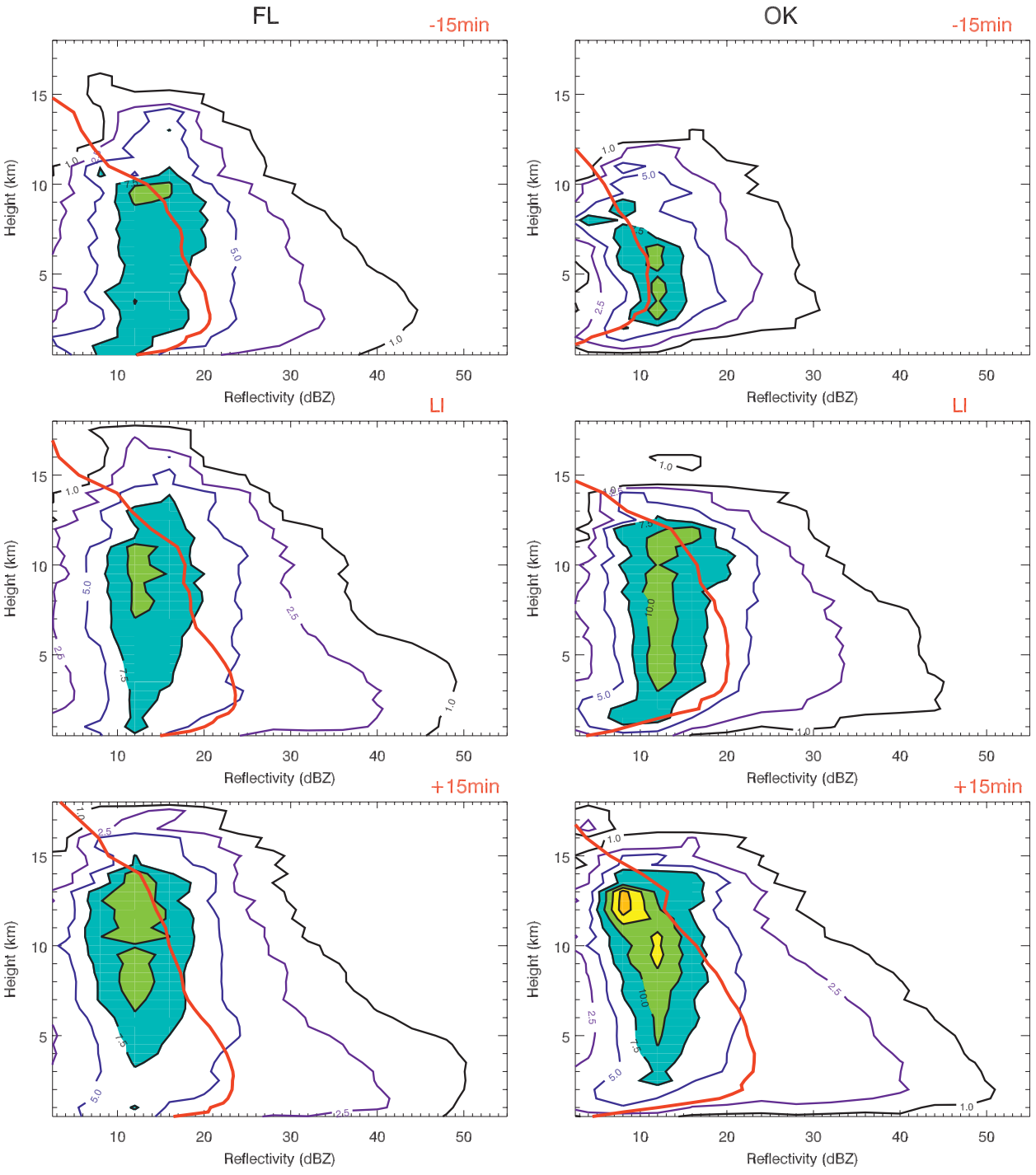

FIG. 1. (*Continued*)

and by the CFADs (Fig. 1). Notch overlap in the 10.7-μm T_B fields occurs at −30 min, at LI, and at +15 min, pointing to significantly different cloud depths in advance of LI between the storms over the two locations. The distributions of cloud growth rates are similar between FL and OK, however, the wider box sizes in OK suggest a tendency for more rapid growth at and before −45 min. The gradual widening of boxes in FL over time, from −45 to +15 min (Fig. 6a), points to clouds being in various growth stages, which is not seen

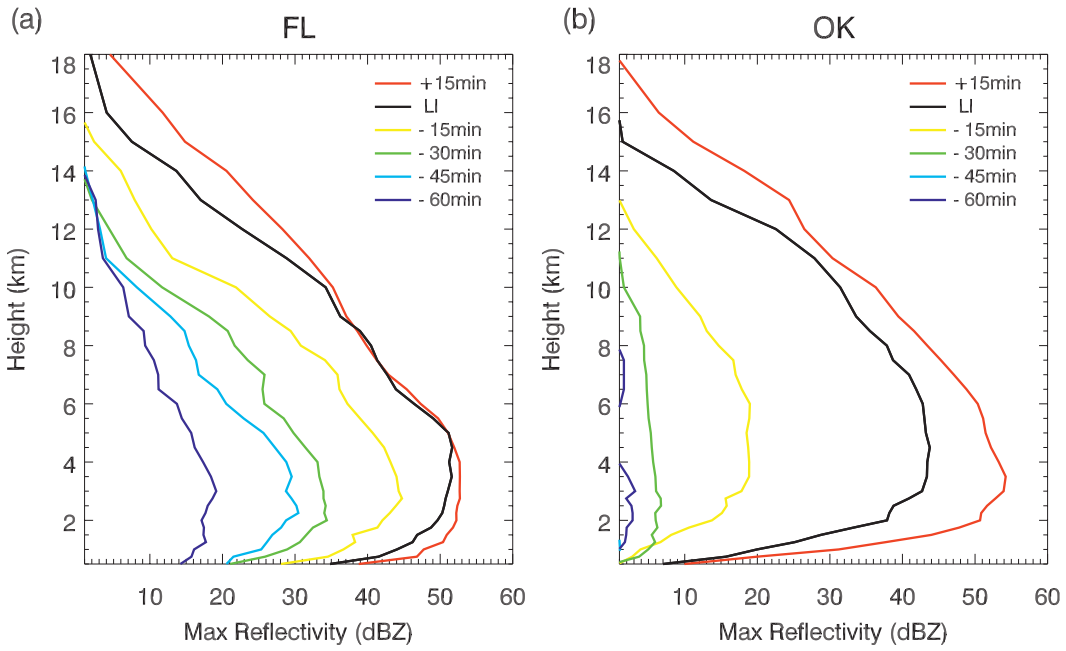

FIG. 2. Maximum reflectivity profiles, every 15 min from −60 min to +15 min, for (a) 36 storms in FL and (b) 23 storms in OK.

in OK. Decreased magnitudes of cloud-top cooling rates after LI in both FL and OK suggest slowing updrafts and anvil development.

Though substantial-to-total notch overlap over the entire period suggests that this field is invariant between regions, differences in spread exist. With higher moisture contents in FL compared to OK (see section 4c), preexisting warm cumulus clouds are generally developing steadily in FL, as seen by overall less variability in the 6.5–10.7-μm difference field and its trend (Figs. 5b and 6b) between −60 and −30 min. Lesser variability in the 6.5–10.7-μm channel difference in FL occurs because the 6.5-μm channel weighting function is mostly above the cloud top (i.e., lower clouds). Specifically, in the presence of higher water vapor (higher PW), the height of the 6.5-μm weighting function is displaced upward, leading to less response in the 6.5-μm T_B until clouds achieve depths into the midtroposphere, above ~600 hPa (Menzel and Purdom 1994). In OK, the 6.5–10.7-μm difference and its trend also indicate that between −60 and −30 min there are fewer signals of active growing cumulus clouds, while clouds are more consistently present in the following 15 min toward LI. A drier environment in OK, coupled to more rapid cloud development, should also lead to more variability in the 6.5–10.7-μm difference. This is because the cumulus clouds are more often observed in the 6.5-μm channel where they are less obscured by the low-level water vapor.

The IFs indicative of early cumulus cloud development (13.3–10.7 μm, Fig. 5c; 3.9–10.7 μm, Fig. 5d) exhibit large similarity between FL and OK, with the distributions of both fields laying mostly on top each other, while the 3.9–10.7-μm difference has a slightly wider spread. The 13.3–10.7-μm differences approach zero and become negative by +15 min, indicating anvil formation, with positive differences otherwise. The trend toward wider box sizes in the 3.9–10.7-μm difference, in FL more than in OK, suggests that clouds are increasing in altitude and size, as expected. The time trends of both fields (Figs. 6c,d), related to cloud growth rates as channel weighting functions (and hence, channel T_Bs), become juxtaposed at high altitudes near cloud tops (Mecikalski and Bedka 2006; H10).

With few IR channels, the main glaciation indicators on *GOES-12* are the 3.9-μm reflectance and its trend (Figs. 6e,f). Cloud-top glaciation as determined from 3.9-μm reflectance is a function of view angle and particle size. With view angles (also a function of zenith angle) being ≤50° in both OK and FL, <9% reflectance is the threshold we will use to infer glaciation (Lindsey et al. 2006, see their Fig. 5). Consideration of the 10.7-μm T_B field (Fig. 5a) and cloud-top cooling rates (Fig. 6a) together with the 3.9-μm reflectance shows that rapid cloud development *upon glaciation* occurs over FL at the time of LI, suggesting that the influence of the latent heat of fusion is noticeable (freezing of a large amount of water drops to increases vertical motion), as large

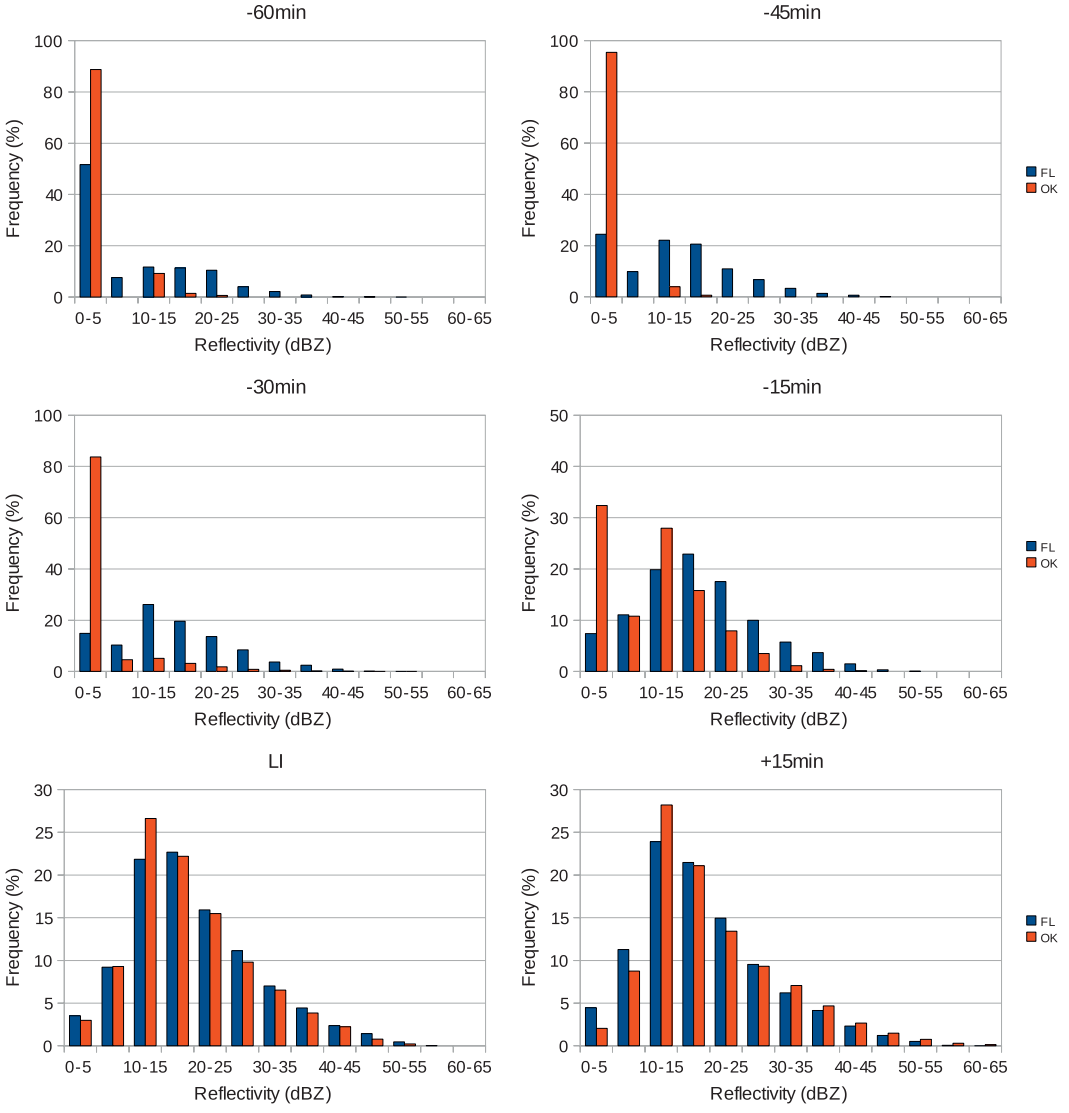

FIG. 3. Reflectivity percentage frequency occurrence, between 0° to −40°C heights with a bin size of 5 dBZ (0–60 dBZ), for the 36 FL storms (blue) and 23 OK storms (red). Plots show LI-relative times from −60 to +15 min. Reflectivity values in the 0–5-dBZ bin are indicative of "clear air," non-precipitation returns, and are shown to highlight the absence of in-cloud hydrometeors or detectable precipitation.

amounts of rain droplets are lofted well above the freezing level by the main updraft. This is seen as the mean 10.7-μm cooling rates sharply decrease in FL to -18°C (15 min)$^{-1}$ at LI [cf. -16°C (15 min)$^{-1}$ in OK]. At this threshold, cloud tops were mostly glaciated in FL by −15 min, and at LI in OK. If the warm rain process is dominant in FL, as the CFAD results suggest, then the water hydrometeors between −60 to −15 min in FL would be lofted, become supercooled, and/or freeze into graupel and hail particles in the mixed-phase layer. The presumption is that these larger particles then contribute substantially to the charging process, if they are imbedded in the main updraft, which possibly explains why LI occurs later in the FL storms relative to the appearance of significant radar echoes. In both regions, cloud growth slows after LI, yet may be more rapid in OK, as the implied stronger updrafts in OK reach an equilibrium level sooner than in FL, while the FL storms in fact achieve higher heights. A discussion on how parcel instability is related to these results is presented below.

One of the interesting aspects is that the 3.9-μm reflectance is higher in OK events in advance of LI. While higher in OK, since view angles were <68° for both locations for all LI events, with all things being equal, the

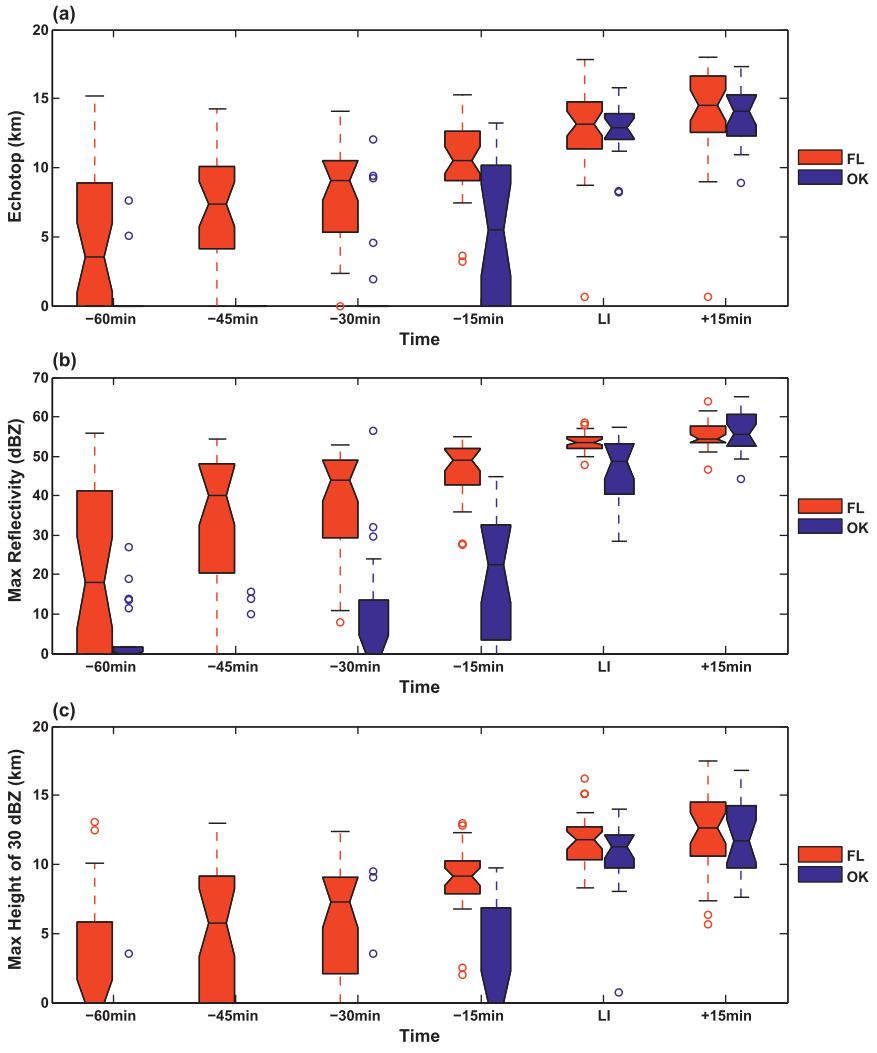

FIG. 4. Box-and-whiskers plots, from −60 to +15 min of radar parameters and comparing the FL (red) and OK (blue) storms, where (a) is the echo top, (b) is the maximum reflectivity, and (c) is the maximum height of 30 dB*Z*. The top and bottom ends of the box are the first and third quartiles. The middle line marks the median. The plot whiskers extend out to 1.5 times the length of the box. The outliers are plotted as the open circles.

percentage differences in 3.9-μm reflectance for glaciated clouds between OK and FL should not be more than 2% (Lindsey et al. 2006). In this light, the 3.9-μm reflectance results suggest that 1) the presence of smaller particles and hence stronger and/or cooler/drier updrafts in OK, where hydrometeors have less time to grow before an updraft reaches the tropopause, results in an abundance of small particles at cloud top leading to higher reflectance. In effect, the small particles in OK freeze later at colder temperatures within stronger updrafts, in light of Rosenfeld and Woodley (2000) and Rosenfeld et al. (2008). 2) Larger particles near cloud top in FL produce lower reflectance in contrast. 3) Cloud development and updraft strengths from storm to storm appear more varied in OK, given larger variability (wider box sizes) in 3.9-μm reflectance data, which is consistent with other trend fields. Also, 4) FL events may possess well-defined anvils with widespread glaciation at LI compared to in OK, as indicated by the very small box sizes (small storm-to-storm variability) from LI to +15 min in FL versus in OK. Therefore, the presence of an anvil in advance of LI may be important information when forecasting first-flash LI in FL. Furthermore, OK storms may have anvils still partly composed of unfrozen hydrometeors, as just discussed, and more overshooting tops (Rosenfeld and Woodley 2000). Referring to point 3, another interpretation of the wider distribution of 3.9-μm reflectance in OK is the presence

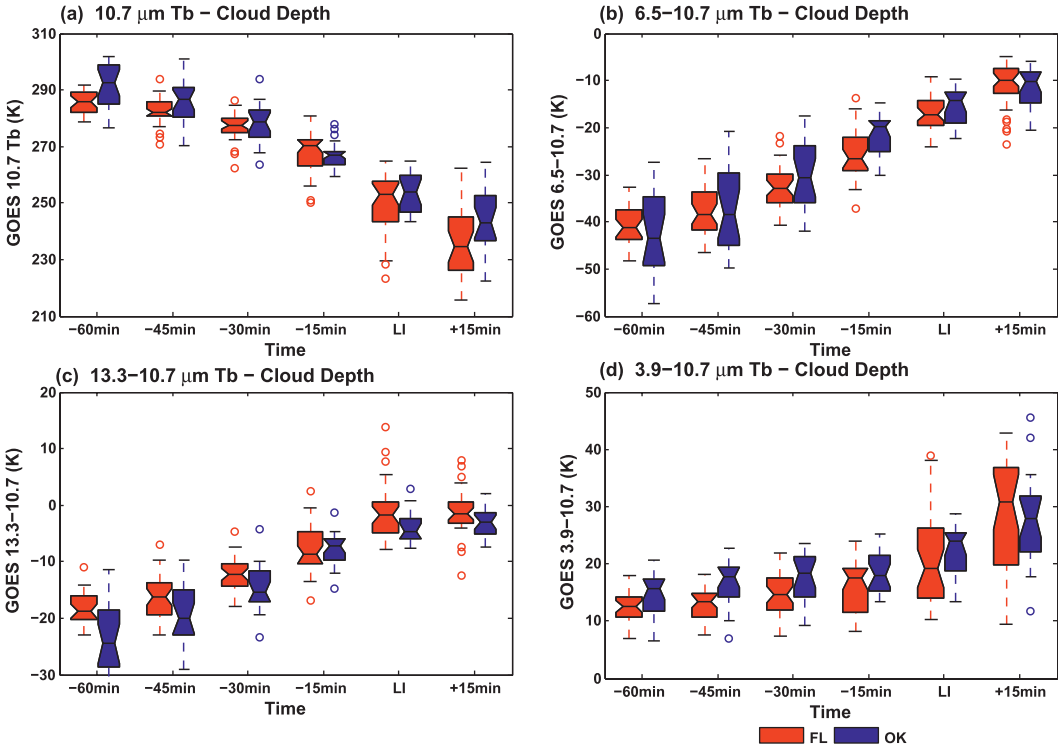

FIG. 5. Box-and-whiskers plots, from −60 to +15 min of *GOES-12* and comparing the FL (red) and OK (blue) storms, where (a) is the 10.7-μm T_B, (b) is the 6.5–10.7-μm T_B difference, (c) is the 13.3–10.7-μm T_B difference, and (d) is the 3.9–10.7-μm T_B difference.

of smaller clouds in the −60- to −15-min period, and hence more influence from surface temperatures within this channel (Ellrod 1995).

Despite the significant differences in the 3.9-μm reflectance, the 3.9-μm reflectance trends (Fig. 6f) share similar patterns between −60 and +15 min in both locations, where again, more variability is seen in OK between −60 and −15 min suggesting cumulus clouds in stages of rapid growth, or smaller clouds, in advance of LI. Finally, the local minimum in the IQR of 3.9-μm reflectance trend between −30 and −15 min at both locations (as discussed in H10) is also prevalent, suggesting that this may also be a strong forecast indicator of first-flash LI.

The GOES-observed storm area increases steadily within the last 30 min before LI for both regions (Fig. 7). The OK storms have larger median values of both storm area and the 15-min upward trend in storm area than FL storms. Storm area is defined as *GOES-12* pixels with 10.7-μm T_B values <273 K. The OK and FL distributions are statistically similar given notch overlap through the period for both fields in Fig. 7. One possible explanation for the larger post-LI storm sizes in OK is the development of wider updrafts and more explosive cloud growth (within a deeper boundary layer with larger instability), which is consistent with the 3.9-μm reflectance and CFAD results. In contrast, the lower mean values of storm area and the 15-min upward trend in storm area in FL suggest that these storms possess slow growth rates with lower magnitudes of anvil-level mass divergence and weaker vertical motions up to the −15-min time.

c. *Environmental factors*

Table 3 lists the RUC sounding parameters averaged over all storm days. As expected, PW values are markedly higher over FL as compared to OK, reaching ~56 mm and with a median value of 52.8 mm. This supports the occurrence of a significant large hydrometeor volume and an early warm rain phase in the developing cumulus clouds analyzed, as confirmed by early stage (−60 to −30 min) signatures of the echo top (Fig. 4a), maximum Z (Fig. 4b), and maximum 30-dBZ height (Fig. 4c). These signatures were generally not seen over OK, within the drier environments (PW values ranging from 35.6–50.6 mm). The LCL and LFC values vary substantially between the two locations, being mainly <1600 m over FL. Over OK, maximum LCL values approach twice that value, and LFCs are similarly much larger. The deeper subcloud/boundary layer supports the likely

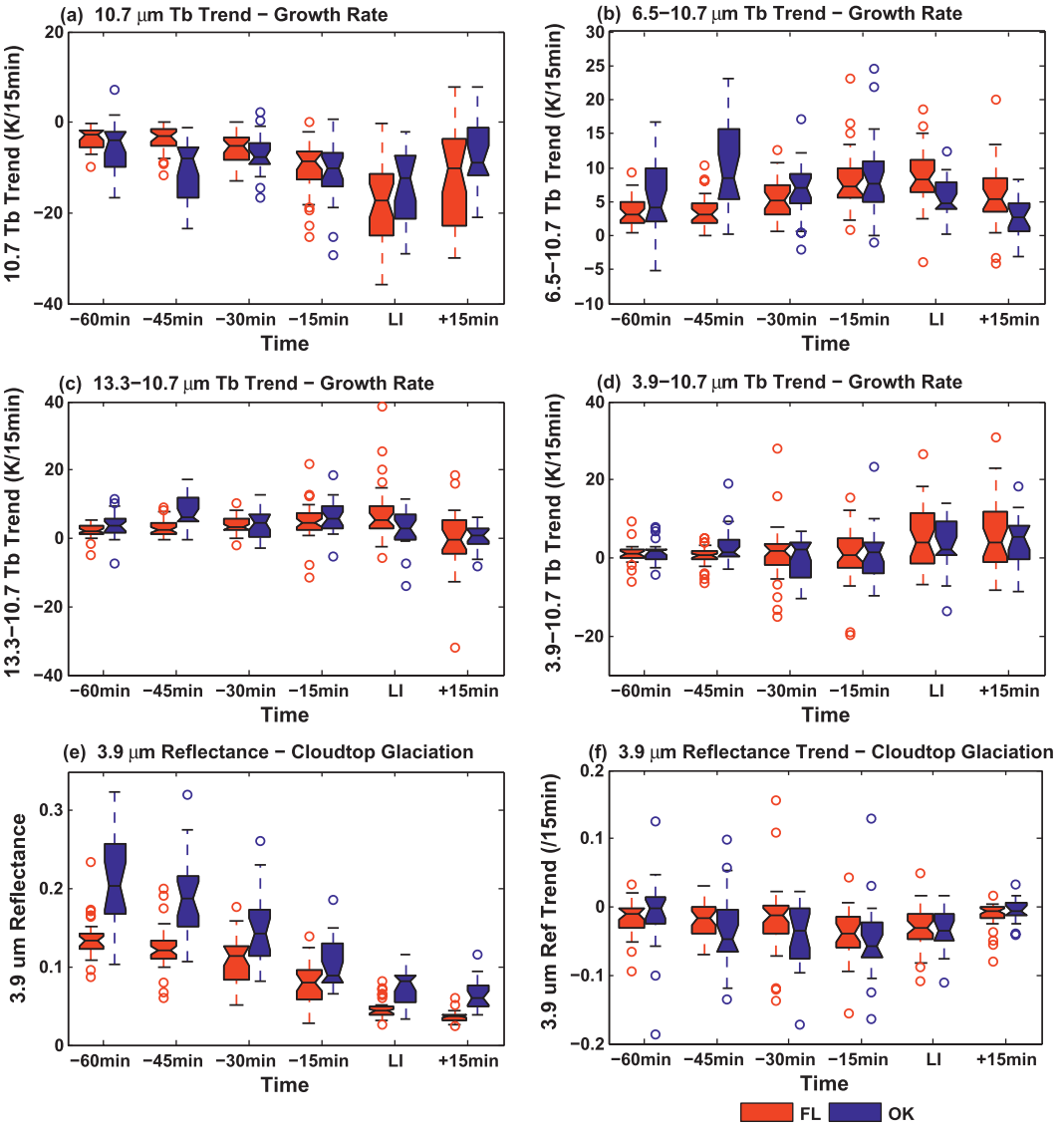

FIG. 6. Box-and-whiskers plots, from −60 to +15 min of *GOES-12* and comparing the FL (red) and OK (blue) storms, where (a) is the 10.7-μm T_B 15-min trend, (b) is the 6.5–10.7-μm T_B difference 15-min trend, (c) is the 13.3–10.7-μm T_B difference 15-min trend, (d) is the 3.9–10.7-μm T_B difference 15-min trend, and (e),(f) are the 3.9-μm reflectance, and 3.9-μm reflectance 15-min trend, respectively.

occurrence of wider updrafts in the OK convective storms, which would lead to stronger signals in the IR fields (as ~4 km × 4 km GOES pixels will be more filled with cumulus clouds), and that CI and LI would occur sooner, relative to the "towering cumulus" stage of storm development, given the presence of a robust in-cloud charging process. Wider updrafts imply less lateral entrainment mixing into a central updraft core, more CAPE realization in terms of updraft strength, and a lofting of larger amounts of hydrometeors, with the implication that storm development is more rapid (Browning 1964, 1965; Goldman 1968; Warner 1970). These factors support the CFAD and GOES IF observations of more rapid in-cloud precipitation echo field and convective cloud developments in OK.

Larger CAPE values in OK also support a more rapid storm development. No significant differences are noted in the FRZLVL or in the mean CIN values, between the two locations, which suggests that the differing rates of storm (radar echo) development, and differences in the 3.9-μm reflectance signals for glaciation, are not significantly influenced by FRZLVL or CIN, respectively. Yet, the distribution of CIN (Fig. 8) shows more negative values in OK, which would have the effect of

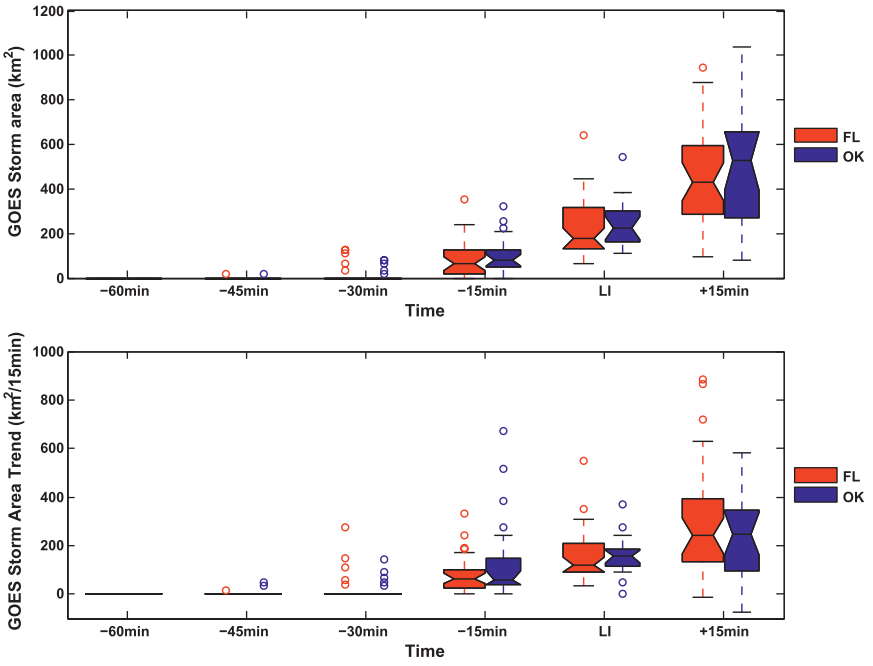

FIG. 7. Box-and-whiskers plots of (top) storm area and (bottom) the 15-min trend, for the FL (red) and OK (blue) storms. Storm area is calculated using all pixels with *GOES-12* 10.7-μm T_B values <273 K.

delaying storm initiation, pointing to more explosive growth as a capping inversion is removed late in the day. The vastly different LCL heights between FL and OK, with similar FRZLVL altitudes, suggest that different precipitation processes are promoted in the two regions. The depth of warm cloud layer, the volume between LCL and FRZLVL (''FRZLVL–LCL''), would average 3621 m for FL and 2256 m for OK. The significantly

TABLE 3. Stability parameters from the Rapid Update Cycle model 0-h analysis fields in the region of thunderstorm development at 0000 UTC. The 0000 UTC sounding is analyzed because it is ''afternoon'' for the days studied (e.g., 0000 UTC 3 Jun applies to the afternoon of 2 Jun). All days, for the lightning initiation events analyzed in this study, are in 2009. Here, ''Lat'' is latitude, ''Lon'' is longitude, ''LCL'' is lifted condensation level, ''LFC'' is level of free convection, ''CBL'' is convective boundary layer, ''PW'' is precipitable water, ''CAPE'' is mean layer convective available potential energy (J kg^{-1}), ''CIN'' is convective inhibition (J kg^{-1}), and ''FRZLVL'' is freezing level. All other units are shown. See Fig. 8 for graphical comparisons.

FL	Lat (°)	Lon (°)	LCL (m)	LFC (m)	CBL Depth (m)	PW (mm)	CAPE	CIN	FRZLVL (m)
2 Jun	28.53	−80.74	743	838	1043	34.54	1392	0	4162
15 Jun	28.51	−81.12	1658	1941	1063	54.36	828	−4	4553
26 Jun	28.87	−81.17	620	2485	1545	52.07	885	−79	4607
12 Jul	28.28	−80.95	963	1417	1631	51.82	1322	−4	4552
18 Jul	28.48	−81.04	521	1414	1522	43.69	1347	−22	4478
29 Jul	28.55	−81.00	1244	1344	1497	54.36	2371	0	4583
30 Jul	28.61	−81.16	1236	1936	1335	56.39	1005	−10	4659
19 Aug	28.38	−81.00	682	1416	1069	50.04	1065	−7	4911
21 Aug	28.31	−81.22	935	1936	1130	53.09	2055	−13	4523
23 Aug	28.75	−81.09	734	1418	1331	53.34	2308	−7	4525
Avg			934	1615	1317	50.4	1458	−15	4555
OK									
25 May	35.09	−96.50	1391	1470	1824	35.56	2392	0	3988
27 Jun	35.01	−97.20	2264	2544	2546	36.58	2589	−4	5110
30 Jun	34.34	−96.92	2171	3103	4025	34.54	1484	−24	4338
1 Jul	34.44	−96.42	1780	2183	1538	45.47	3042	−6	4416
16 Jul	34.99	−97.01	871	2514	1594	50.55	2732	−106	4732
10 Aug	35.15	−97.07	1584	1969	2992	48.77	2832	−7	4736
Avg			1677	2297	2420	41.9	2512	−21	4553

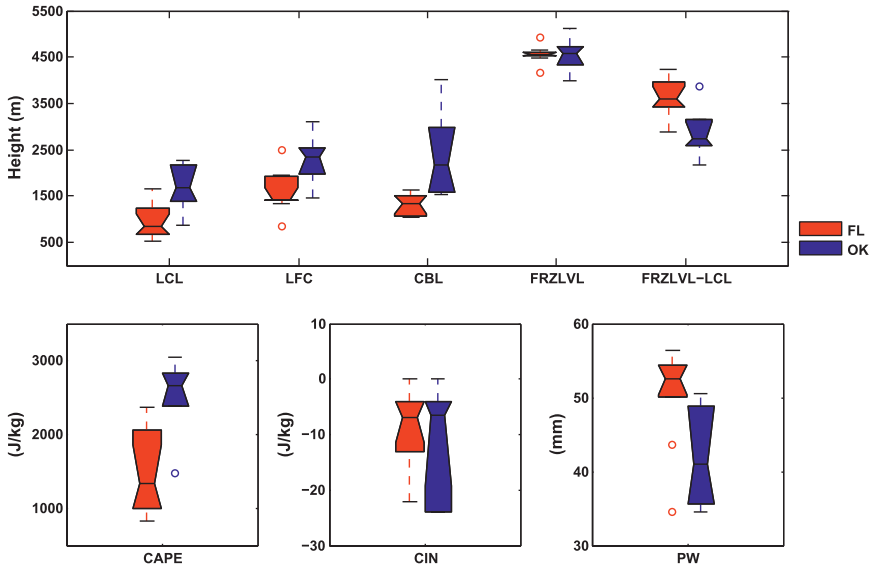

FIG. 8. Box-and-whiskers plots showing the distribution of environmental variable for FL (red) and OK (blue) on days when the LI events were analyzed. See Table 3 for a description of the labeled variables, and see the text for a discussion.

larger volume of warm cloud (60.5% greater, with a lower LCL) in FL is more conducive to warm rain production, consistent with the CFAD analysis. In comparison, stronger and more explosive growing updrafts in OK storms give limited time for condensation and coalescence growth. Combined with a shallower warm cloud layer, much less warm rain is produced in OK storms, with the opposite occurring in the FL LI events.

5. Discussion and conclusions

The forecast of the onset of lightning within convective clouds remains a challenging problem. Because of the involvement of small-scale lightning charging processes, the average lead time for LI is about 10–20 min (Yang and King 2010; Mosier et al. 2011) when radar Z data are used alone, and can be up to ~1 h in some cases when GOES IF indicators are used independently (H10). As a follow-up to H10, this study examines GOES IR IFs in concert with radar Z datasets for LI events, from 60 min in advance of LI to 15 min after LI, as a means of increasing understanding of satellite–radar relationships, and developing a more solid predictive capability for the first-flash LI. Another purpose is enhancing understanding of in-cloud physical processes when time series of Z and IR satellite data are analyzed coincidently in advance of LI for newly growing convective storms. Lightning-producing thunderstorms in two different geographical regions (36 in FL and 23 in OK) during the 2009 summer are analyzed in CFADs using 3D NMQ Z data, 10 *GOES-12* IR IFs, RUC model sounding-based moisture/PW, and boundary layer and thermodynamic variables. The CFADs are developed following studies of Wang and Carey (2005) and Cecil (2011).

Radar CFAD coupled to GOES IF analyses indicate that the characteristics of OK storms differ significantly from the FL storms. Overall, the main results are summarized as follows:

1) It takes a longer time to prepare and grow the large ice in the mixed layer hydrometeor field in lightning-active FL storms, beginning with a dominant "warm rain" process in FL. The presumption, based on previous research (Jameson et al. 1996; Ramachandran et al. 1996; Bringi et al. 1997) and as observed here, is that the 1–5-km altitude warm rain in FL is subsequently lofted to become a larger portion of the mixed-phase region of the cloud, where these particles freeze and then participate in the charging process. A deep warm layer (i.e., FRZLVL–LCL depths) supports an active warm rain process in FL, averaging 3621 m in FL versus only 2256 m in OK.
2) The OK storms develop more abruptly before LI. Rapid growth is found at both locations at the LI time. Without the warm rain process being consistently active in OK, the analysis suggests that the main updrafts in OK are wider and drier, and hence mixed-phase hydrometeor fields form later and more abruptly above the FRZLVL altitude, beginning only ~30 min in advance of LI. We infer that, from the freezing of large hydrometeor volumes in the

more moist FL storms, the latent heat of fusion contributes significantly to updraft strengths in the −15 min to LI time frame.

3) From the *GOES-12* IFs, the faster cloud growth over OK between −60 and −15 min, as seen in the 10.7-μm T_B cooling rate and 3.9-μm reflectance trend (and to some extent the 6.5–10.7-μm trend) fields, is consistent with the higher CAPE values in this location (averaging 2512 in OK vs 1458 in FL). As noted, there appears to be an updraft-strength-related signature in FL associated with the freezing of the large amount of hydrometeors, beginning within the last 15 min before LI, which is also seen in the 6.5–10.7-μm trend field.
4) The lower PW and higher CAPE values in OK are accompanied by higher 3.9-μm reflectance in the pre-LI clouds, where the associated relationship is that stronger and slightly drier updrafts produce a greater abundance of small particles that freeze later, keeping the cloud-top reflectance higher than FL (where PW values are higher and CAPE values are lower); the caveat here is that reflectance may be ~2% larger in OK compared to FL simply because of larger view angles in OK (Lindsey et al. 2006), along the lines of Rosenfeld et al. (2008) and Lensky and Rosenfeld (2008). CFAD fields in OK at +15 min are consistent with the presence of large percentage fractions of small ice particles in the 10.5- to ~15-km layer, unlike in FL.
5) From *GOES-12* and CFAD data, clouds in the −60- to −30-min period over OK are far less developed, also in terms of their hydrometeor (Z) fields, which is reflected as more variability (i.e., wider box sizes) than over FL (e.g., in the 6.5–10.7-μm difference, in the 13.3–10.7-μm difference, and 3.9-μm reflectance).
6) The 3.9–10.7-μm difference, and the 15-min 13.3–10.7-μm and 3.9–10.7-μm time trends appear to provide little unique information for discerning physical process differences between OK and FL, all showing similarly consistent patterns associated with growing cumulus clouds. H10 noted that the 15-min 3.9–10.7-μm trend did not provide much unique information when nowcasting LI. However, similar to H10, the 3.9-μm reflectance trend does show a subtle decrease–increase signature in the −30 min to LI time frame, which may have forecast value when nowcasting LI, yet this local minimum may not be statistically significant (robust) given notch overlap between −15 and +15 min in Fig. 6f.

Related to points 1–4, the signatures seen in the GOES and CFAD Z fields are consistent with the results presented in Rosenfeld and Lensky (1998), Khain et al. (2001), and to some extent Khain et al. (2005), in which updraft strengths directly influence hydrometeor particle sizes, and therefore cloud-top signatures observed by geostationary satellite imagery (GOES, in particular). Particle growth rates and sizes are a function of time spent within low-altitude portions of clouds where moisture contents are the highest. An inverse relationship is found between updraft strength (e.g., measured in 15 min 10.7-μm and 6.5–10.7-μm trends) and particle sizes, which are subsequently linked to instability (CAPE as related to vertical motion). Small ice particles at the cloud top produce relatively high 3.9-μm reflectance, and vice versa. The depth of the >0°C layer in clouds may complicate these updraft strength–particle size relationships by regulating how rapidly particles grow at low levels (below the FRZLVL) if the updrafts are strong. Yet, between FL and OK, the effects on regulating particle sizes are magnified as slower-updraft storms in FL growing in lower CAPE environments are also subject to robust warm rain processes (autoconversion, collection; e.g., Kessler 1969), further increasing particle sizes.

In terms of forecasting the occurrence of the first lightning flash (of any kind, whether IC, CG, cloud-to-air, or cloud-to-cloud), this study offers new insights. From our analysis, and as a follow-on to H10, the time elapsed for LI occurrence, in conjunction with CI or after, is on the order of 30–60 min for FL storms, whereas it may be only 10–15 min for OK storms, regardless of whether radar and/or satellite fields are evaluated (albeit satellite dataset provide the longest forecast lead times). As strong radar echoes need to be present to be used as a predictor of LI in most current studies (e.g., Yang and King 2010; Mosier et al. 2011), Z data only offer a maximum of ~10–20-min lead times for the occurrence of first lightning flash. Therefore, using radar and geostationary satellite data *together* for LI nowcasting would be helpful toward the following: 1) exploiting the 30–60-min lead time provided by geostationary satellites and 2) constraining the satellite-only predictions by the need to have a specific in-cloud radar Z signature present ahead of making a high-probability (> ~80%) LI nowcast. This should lead to lower false-alarm rates in purely satellite-based CI and LI nowcasts, and longer lead times beyond using radar data alone. The specific coupled CFAD–GOES signature, which shows promise when nowcasting LI, is the presence of a well-defined anvil in FL (or in similar environments) with a concomitant drop off in cloud-top cooling rates.

For follow-on research, this study only uses a small dataset. Further analysis should be conducted with more cases based on similar criteria to confirm the conclusions and to clarify whether the differences seen are not case,

regime, or seasonally dependent. Areas of new research can also include relating the GOES and CFAD datasets to lightning intensity (in terms of flash density; see McCaul et al. 2009) such that predictions of lightning amounts and rates may be made with higher accuracy. Use of geostationary sensors with more than four broad band channels, such as the MSG, the Fengyun series, and the forthcoming GOES-R/-S, have already been demonstrated to provide benefit when discerning in–cloud physical processes in advance of CI (Mecikalski et al. 2010a,b), and therefore should be coupled to radar datasets toward gaining additional understanding on how LI may be properly forecasted.

Acknowledgments. This work was supported by the National Science Foundation (NSF) Grant ATM-0813603. The authors thank Dr. Carrie Langston for valuable help with processing the NOAA National Mosaic and Multi-sensor QPE (NMQ) dataset, and Captain Ryan Harris for processing the *GOES-12* lightning-initiation focused data, which were relied upon in this effort. Three anonymous reviewers (one especially) provided considerable direction on how this research article was eventually structured.

REFERENCES

Anderson, H., 2010: Characteristics of decaying storms during lightning cessation at Kennedy Space Center and Cape Canaveral Air Force station. M.S. thesis, Florida State University, 62 pp.

Aufdermauer, A. N., and D. A. Johnson, 1972: Change separation due to riming in an electric field. *Quart. J. Roy. Meteor. Soc.,* **98,** 369–382.

Boccippio, D. J., S. J. Goodman, and S. Heckman, 2000: Regional differences in tropical lightning distributions. *J. Appl. Meteor.,* **39,** 2231–2248.

Bringi, V. N., K. Knupp, A. Detwiler, L. Liu, I. J. Caylor, and R. A. Black, 1997: Evolution of a Florida thunderstorm during the Convection and Precipitation/Electrification Experiment: The case of 9 August 1991. *Mon. Wea. Rev.,* **125,** 2131–2160.

Browning, K. A., 1964: Airflow and precipitation trajectories within severe local storms which travel to the right of the mean wind. *J. Atmos. Sci.,* **21,** 634–639.

——, 1965: Some inferences about the updraft within a severe local storm. *J. Atmos. Sci.,* **22,** 669–677.

——, and D. Atlas, 1965: Initiation of precipitation in vigorous convective clouds. *J. Atmos. Sci.,* **22,** 678–683.

Buechler, D. E., and S. J. Goodman, 1990: Echo size and asymmetry: Impact on NEXRAD storm identification. *J. Appl. Meteor.,* **29,** 962–969.

Carey, L. D., and S. A. Rutledge, 1996: A multiparameter radar case study of the microphysical and kinematic evolution of a lightning–producing storm. *Meteor. Atmos. Phys.,* **59,** 33–64.

——, and ——, 2000: On the relationship between precipitation and lightning in tropical island convection: A C-band polarimetric radar study. *Mon. Wea. Rev.,* **128,** 2687–2710.

Cecil, D. J., 2011: Relating passive 37-GHz scattering to radar profiles in strong convection. *J. Appl. Meteor. Climatol.,* **50,** 233–240.

——, and E. J. Zipser, 2002: Reflectivity, ice scattering, and lightning characteristics of hurricane eyewalls and rainbands. Part II: Intercomparison of observations. *Mon. Wea. Rev.,* **130,** 785–801.

——, S. J. Goodman, D. J. Boccippio, E. J. Zipser, and S. W. Nesbitt, 2005: Three years of TRMM precipitation features. Part I: Radar, radiometric, and lightning characteristics. *Mon. Wea. Rev.,* **133,** 543–566.

Deierling, W., and W. A. Petersen, 2008: Total lightning activity as an indicator of updraft characteristics. *J. Geophys. Res.,* **113,** D16210, doi:10.1029/2007JD009598.

——, ——, J. Latham, S. Ellis, and H. J. Christian, 2008: The relationship between lightning activity and ice fluxes in thunderstorms. *J. Geophys. Res.,* **113,** D15210, doi:10.1029/2007JD009700.

Del Genio, A. D., and W. Kovari, 2002: Climatic properties of precipitating convection under varying environmental conditions. *J. Climate,* **15,** 2597–2615.

desJardins, M. L., K. F. Brill, and S. S. Schotz, 1991: Use of GEMPAK on UNIX workstations. Preprints, *Seventh Int. Conf. on Interactive, Information and Processing Systems for Meteorology, Oceanography, and Hydrology,* New Orleans, LA, Amer. Meteor. Soc., 449–453.

Dye, J. E., J. J. Jones, A. J. Weinheimer, and W. P. Winn, 1988: Observations within two regions of charge during initial thunderstorm electrification. *Quart. J. Roy. Meteor. Soc.,* **114,** 1271–1290.

——, W. P. Winn, J. J. Jones, and D. W. Breed, 1989: The electrification of New Mexico thunderstorms. Part I: Relationship between precipitation development and the onset of electrification. *J. Geophys. Res.,* **94,** 8643–8656.

Ellrod, G. P., 1995: Advances in the detection and analysis of fog at night using GOES multispectral infrared imagery. *Wea. Forecasting,* **10,** 606–619.

Elster, J., and H. Geitel, 1913: Zur Influenztheorie der Niederschlagselektrizitaet (On the influence theory of precipitation electricity). *Phys. Z.,* **14,** 1287–1292.

Emersic, C., and C. P. R. Saunders, 2010: Further laboratory investigations into the relative diffusional growth rate theory of thunderstorm electrification. *Atmos. Res.,* **98,** 327–340.

Goldman, J. L., 1968: The high speed updraft: The key to the severe thunderstorm. *J. Atmos. Sci.,* **25,** 222–248.

Goodman, S. J., D. E. Buechler, and P. J. Meyer, 1988: Convective tendency images derived from a combination of lightning and satellite data. *Wea. Forecasting,* **3,** 173–188.

Gremillion, M. S., and R. E. Orville, 1999: Thunderstorm characteristics of cloud-to-ground lightning at the Kennedy Space Center, Florida: A study of lightning initiation signatures as indicated by the WSR-88D. *Wea. Forecasting,* **14,** 640–649.

Harris, R. J., J. R. Mecikalski, W. M. MacKenzie, P. A. Durkee, and K. E. Nielsen, 2010: The definition of GOES infrared lightning initiation interest fields. *J. Appl. Meteor. Climatol.,* **49,** 2527–2543.

Helsdon, J. H., Jr., S. Gattaleeradapan, R. D. Farley, and C. C. Waits, 2002: An examination of the convective charging hypothesis: Charge structure, electric fields, and Maxwell currents. *J. Geophys. Res.,* **107,** 4630, doi:10.1029/2001JD001495.

Hinson, M. S., 1997: A study of the characteristics of thunderstorm cessation at the NASA Kennedy Space Center. M.S. thesis, Texas A&M University, College Station, TX, 91 pp.

Hondl, K. D., and M. D. Eilts, 1994: Doppler radar signatures of developing thunderstorms and their potential to indicate the

onset of cloud-to-ground lightning. *Mon. Wea. Rev.,* **122,** 1818–1836.

Jameson, A. R., M. J. Murphy, and E. P. Krider, 1996: Multiple–parameter radar observations of isolated Florida thunderstorms during the onset of electrification. *J. Appl. Meteor.,* **35,** 343–354.

Katsanos, D. K., K. Lagouvardos, V. Kotroni, and A. A. Argiriou, 2007: The relationship of lightning activity with microwave brightness temperatures and spaceborne radar reflectivity profiles in the central and eastern Mediterranean. *J. Appl. Meteor. Climatol.,* **46,** 1901–1912.

Kessler, E., III, 1969: *On the Distribution and Continuity of Water Substance in Atmospheric Circulations. Meteor. Monogr.,* No. 32, Amer. Meteor. Soc., 84 pp.

Khain, A. P., D. Rosenfeld, and A. Pokrovsky, 2001: Simulating convective clouds with sustained supercooled liquid water down to −37.5°C using a spectral microphysics model. *Geophys. Res. Lett.,* **28** (20), 3887–3890.

——, ——, and ——, 2005: Aerosol impact on the dynamics and microphysics of convective clouds. *Quart. J. Roy. Meteor. Soc.,* **131,** 1–25.

Krehbiel, P. R., R. J. Thomas, W. Rison, T. Hamlin, J. Harlin, and M. Davis, 2000: GPS-based mapping system reveals lightning inside storms. *Eos, Trans. Amer. Geophys. Union,* **81,** 21–25.

Lau, K. M., and H. T. Wu, 2003: Warm rain processes over tropical oceans and climate implications. *Geophys. Res. Lett.,* **30,** 2290, doi:10.1029/2003GL018567.

Lensky, I. M., and D. Rosenfeld, 2008: Clouds–Aerosols–Precipitation Satellite Analysis Tool (CAPSAT). *Atmos. Chem. Phys.,* **8,** 6739–6753.

Lindsey, D. T., D. W. Hillger, L. Grasso, J. A. Knaff, and J. F. Dostalek, 2006: GOES climatology and analysis of thunderstorms with enhanced 3.9-μm reflectivity. *Mon. Wea. Rev.,* **134,** 2342–2353.

Liu, C., E. J. Zipser, D. J. Cecil, S. W. Nesbitt, and S. Sherwood, 2008: A cloud and precipitation feature database from nine years of TRMM observations. *J. Appl. Meteor. Climatol.,* **47,** 2712–2728.

——, E. R. Williams, E. J. Zipser, and G. Burns, 2010: Diurnal variations of global thunderstorms and electrified shower clouds and their contribution to the global electrical circuit. *J. Atmos. Sci.,* **67,** 309–323.

MacGorman, D. R., and W. D. Rust, 1998: *The Electrical Nature of Storms*. Oxford University Press, 422 pp.

Mansell, E. R., D. R. MacGorman, C. L. Ziegler, and J. M. Straka, 2005: Charge structure and lightning sensitivity in a simulated multicell thunderstorm. *J. Geophys. Res.,* **110,** D12101, doi:10.1029/2004JD005287.

McCaul, E. W., Jr., S. J. Goodman, K. M. LaCasse, and D. J. Cecil, 2009: Forecasting lightning threat using cloud–resolving model simulations. *Wea. Forecasting,* **24,** 709–729.

Mecikalski, J. R., and K. M. Bedka, 2006: Forecasting convective initiation by monitoring the evolution of moving cumulus in daytime GOES imagery. *Mon. Wea. Rev.,* **134,** 49–78.

——, S. J. Paech, K. M. Bedka, and L. A. Litten, 2008: A statistical evaluation of GOES cloud-top properties for nowcasting convective initiation. *Mon. Wea. Rev.,* **136,** 4899–4914.

——, W. M. Mackenzie, M. König, and S. Muller, 2010a: Cloud-top properties of growing cumulus prior to convective initiation as measured by Meteosat Second Generation. Part I: Infrared fields. *J. Appl. Meteor. Climatol.,* **49,** 521–534.

——, ——, ——, and ——, 2010b: Cloud-top properties of growing cumulus prior to convective initiation as measured by Meteosat Second Generation. Part II: Use of visible reflectance. *J. Appl. Meteor. Climatol.,* **49,** 2544–2558.

Menzel, W. P., and J. F. Purdom, 1994: Introducing GOES-I: The first of a new generation of geostationary operational environmental satellites. *Bull. Amer. Meteor. Soc.,* **75,** 757–781.

Michimoto, K., 1991: A study of radar echoes and their relation to lightning discharge of thunderclouds in the Hokuriku District. Part I: Observation and analysis of thunderclouds in summer and winter. *J. Meteor. Soc. Japan,* **69,** 327–335.

——, 1993: A study of radar echoes and their relation to lightning discharges of thunderclouds in the Hokuriku district. Part II: Observation and analysis of ''single-flash'' thunderclouds in midwinter. *J. Meteor. Soc. Japan,* **71,** 195–204.

Mitzeva, R. P., C. P. R. Saunders, and B. Tsenova, 2005: A modeling study of the effect of cloud saturation and particle growth rates on charge transfer in thunderstorm electrification. *Atmos. Res.,* **76,** 206–221.

Mosier, R. M., C. Schumacher, R. E. Orville, and L. D. Carey, 2011: Radar nowcasting of cloud–to–ground lightning over Houston, Texas. *Wea. Forecasting,* **26,** 199–212.

Murphy, M. J., K. L. Cummins, N. W. S. Demetriades, and W. P. Roeder, 2008: Performance of the new Four-Dimensional Lightning Surveillance System (4DLSS) at the Kennedy Space Center/Cape Canaveral Air Force Station complex. Preprints, *13th Conf. on Aviation, Range and Aerospace Meteorology,* New Orleans, LA, Amer. Meteor. Soc., 8.6. [Available online at https://ams.confex.com/ams/88Annual/techprogram/paper_131130.htm.]

Nelson, L. A., 2002: Synthesis of 3-dimensional lightning data and weather radar data to determine the distance that naturally occurring lightning travels from thunderstorms. M.S. thesis, Dept. of Engineering Physics, Air Force Institute of Technology, 85 pp.

Nelson, L. D., 1971: A numerical study on the initiation of warm rain. *J. Atmos. Sci.,* **28,** 752–762.

Ogura, Y., and T. Takahash, 1973: The development of warm rain in a cumulus model. *J. Atmos. Sci.,* **30,** 262–277.

Pessi, A. T., and S. Businger, 2009: Relationships among lightning, precipitation, and hydrometeor characteristics over the North Pacific Ocean. *J. Appl. Meteor. Climatol.,* **48,** 833–848.

Petersen, W. A., and S. A. Rutledge, 2001: Regional variability in tropical convection: Observations from TRMM. *J. Climate,* **14,** 3566–3586.

——, S. W. Nesbitt, R. J. Blakeslee, R. Cifelli, P. Hein, and S. A. Rutledge, 2002: TRMM observations of intraseasonal variability in convective regimes over the Amazon. *J. Climate,* **15,** 1278–1294.

——, H. J. Christian, and S. A. Rutledge, 2005: TRMM observations of the global relationship between ice water content and lightning. *Geophys. Res. Lett.,* **32,** L14819, doi:10.1029/2005GL023236.

Ramachandran, R., A. Detwiler, J. Helsdon Jr., P. L. Smith, and V. N. Bringi, 1996: Precipitation development and electrification in Florida thunderstorm cells during Convection and Precipitation/Electrification Project. *J. Geophys. Res.,* **101** (D1), 1599–1619.

Roberts, R. D., and S. Rutledge, 2003: Nowcasting storm initiation and growth using *GOES-8* and WSR-88D data. *Wea. Forecasting,* **18,** 562–584.

Roohr, P. B., and T. H. Vonder Haar, 1994: A comparative analysis of the temporal variability of lightning observation and GOES imagery. *J. Appl. Meteor.,* **33,** 1271–1290.

Rosenfeld, D., and I. M. Lensky, 1998: Satellite-based insights into precipitation formation processes in continental and maritime convective clouds. *Bull. Amer. Meteor. Soc.,* **79,** 2457–2476.

——, and W. L. Woodley, 2000: Deep convective clouds with sustained supercooled water down to –37.5 °C. *Nature,* **405,** 440–441.

——, ——, A. Lerner, G. Kelman, and D. T. Lindsey, 2008: Satellite detection of severe convective storms by their retrieved vertical profiles of cloud particle effective radius and thermodynamic phase. *J. Geophys. Res.,* **113,** D04208, doi:10.1029/2007JD008600.

Rutledge, S. A., E. R. Williams, and T. D. Keenan, 1992: The Down Under Doppler and Electricity Experiment (DUNDEE): Overview and preliminary results. *Bull. Amer. Meteor. Soc.,* **73,** 3–16.

Seroka, G. N., R. E. Orville, and C. Schumacher, 2012: Radar nowcasting of total lightning over the Kennedy Space Center. *Wea. Forecasting,* **27,** 189–204.

Siewert, C., 2008: Nowcasting lightning initiation through the use of infrared observations from the GOES satellite. M.S. thesis, Atmospheric Science Department, University of Alabama in Huntsville, 105 pp.

Simpson, S. G., and F. J. Scrase, 1937: The distribution of electricity in thunderclouds. *Proc. Roy. Soc. London,* **161,** 309–352.

Stano, G. T., H. E. Fuelberg, and W. P. Roeder, 2010: Developing empirical lightning cessation forecast guidance for the Cape Canaveral Air Force Station and Kennedy Space Center. *J. Geophys. Res.,* **115,** D09205, doi:10.1029/2009JD013034.

Steiger, S. M., R. E. Orville, and L. D. Carey, 2007a: Total lightning signatures of thunderstorm intensity over north Texas. Part I: Supercells. *Mon. Wea. Rev.,* **135,** 3281–3302.

——, ——, and ——, 2007b: Total lightning signatures of thunderstorm intensity over north Texas. Part II: Mesoscale convective systems. *Mon. Wea. Rev.,* **135,** 3303–3324.

Takahashi, T., 1978: Riming electrification as a charge generation mechanism in thunderstorms. *J. Atmos. Sci.,* **35,** 1536–1548.

Toracinta, E. R., D. J. Cecil, E. J. Zipser, and S. W. Nesbitt, 2002: Radar, passive microwave, and lightning characteristics of precipitating systems in the tropics. *Mon. Wea. Rev.,* **130,** 802–824.

Vincent, B. R., L. D. Carey, D. Schneider, K. Keeter, and R. Gonski, 2004: Using WSR–88D reflectivity data for the prediction of cloud–to–ground lightning: A central North Carolina study. *Natl. Wea. Dig.,* **27,** 35–44.

Wang, J.-J., and L. D. Carey, 2005: The development and structure of an oceanic squall–line system during the South China Sea Monsoon Experiment. *Mon. Wea. Rev.,* **133,** 1544–1561.

Warner, J., 1970: The microstructure of cumulus cloud. Part III: The nature of the updraft. *J. Atmos. Sci.,* **27,** 682–688.

Wilks, D. S., 2011: *Statistical Methods in the Atmospheric Sciences*. 3rd ed. Academic Press, 676 pp.

Williams, E. R., 1988: The electrification of thunderstorms. *Sci. Amer.,* **259,** 48–65.

——, and R. M. Lhermitte, 1983: Radar tests of the precipitation hypothesis for thunderstorm electrification. *J. Geophys. Res.,* **88** (C15), 10 984–10 992.

Wilson, C. T. R., 1916: On some determinations of the sign and magnitude of electric discharges in lighting flashes. *Proc. Roy. Soc. London,* **92,** 555–574.

Wilson, J. W., and W. E. Schreiber, 1986: Initiation of convective storms by radar–observed boundary layer convergent lines. *Mon. Wea. Rev.,* **114,** 2516–2536.

——, G. B. Foote, N. A. Crook, J. C. Fankhauser, C. G. Wade, J. D. Tuttle, C. K. Mueller, and S. K. Kruger, 1992: The role of boundary–layer convergence zones and horizontal rolls in the initiation of thunderstorms: A case study. *Mon. Wea. Rev.,* **120,** 1785–1815.

Wolf, P., 2007: Anticipating the initiation, cessation, and frequency of cloud-to-ground lightning, utilizing WSR-88D reflectivity data. *Natl. Wea. Assoc. Electron. J. Oper. Meteor.,* 2007-EJ1, 19 pp. [Available online at http://www.nwas.org/ej/pdf/2007-EJ1.pdf.]

Woodard, C. J., L. D. Carey, W. A. Petersen, and W. P. Roeder, 2012: Operational utility of dual-polarimetric variables in lightning initiation forecasting. *Electron. J. Oper. Meteor.,* **13** (6), 79–102.

Workman, E. J., and S. E. Reynolds, 1949: Electrical activity as related to thunderstorm cell growth. *Bull. Amer. Meteor. Soc.,* **30,** 142–149.

Xu, W., E. J. Zipser, and C. Liu, 2009: Rainfall characteristics and convective properties of mei-yu precipitation systems over South China, Taiwan, and the South China Sea. Part I: TRMM observations. *Mon. Wea. Rev.,* **137,** 4261–4275.

Yang, Y. H., and P. King, 2010: Investigating the potential of using radar echo reflectivity to nowcast cloud–to–ground lightning initiation over Southern Ontario. *Wea. Forecasting,* **25,** 1235–1248.

Yuter, S. E., and R. A. Houze, 1995: Three-dimensional kinematic and microphysical evolution of Florida cumulonimbus. Part II: Frequency distributions of vertical velocity, reflectivity, and differential reflectivity. *Mon. Wea. Rev.,* **123,** 1941–1963.

Zhang, J., K. Howard, and S. Wang, 2006: Single radar Cartesian grid and adaptive radar mosaic system. Preprints, *12th Conf. on Aviation, Range, and Aerospace Meteorology*, Atlanta, GA, Amer. Meteor. Soc., 1.8.

——, and Coauthors, 2011: National Mosaic and Multi-sensor QPE (NMQ) system:–Description, results and future plans. *Bull. Amer. Meteor. Soc.,* **92,** 1321–1338.

Zipser, E. J., and K. R. Lutz, 1994: The vertical profile of radar reflectivity of convective cells: A strong indicator of storm intensity and lightning probability? *Mon. Wea. Rev.,* **122,** 1751–1759.